The Cryosphere Discuss., 9, 4625–4660, 2015
www.the-cryosphere-discuss.net/9/4625/2015/
doi:10.5194/tcd-9-4625-2015

The Cryosphere Discussions
Open Access

Extraordinary runoff from the Greenland Ice Sheet in 2012 amplified by hypsometry and depleted firn-retention

A. B. Mikkelsen[1,2], A. Hubbard[3,4], M. MacFerrin[5], J. Box[6], S. Doyle[4], A. Fitzpatrick[4], B. Hasholt[1], and H. Bailey[4]

[1]Department of Geosciences and Natural Resource Management, University of Copenhagen, Copenhagen, Denmark
[2]Centre for Permafrost (CENPERM), University of Copenhagen, Øster Voldgade 10, Copenhagen, 1350, Denmark
[3]Centre for Arctic Gas Hydrate, Environment and Climate, Department of Geology, University of Tromsø, Dramsveien 201, 9037, Norway
[4] Department of Geography and Earth Sciences, Aberystwyth University, Aberystwyth, SY23 3DB, UK
[5]Cooperative Institute for Research in Environmental Sciences (CIRES), University of Colorado, Boulder, CO, USA
[6]Department of Marine Geology and Glaciology, Geological Survey of Denmark and Greenland, Copenhagen, Denmark

Received: 21 July 2015 – Accepted: 29 July 2015 – Published: 3 September 2015

Correspondence to: A. B. Mikkelsen (bechmikkelsen@gmail.com)

Published by Copernicus Publications on behalf of the European Geosciences Union.

TCD
9, 4625–4660, 2015

Abstract

It has been argued that the infiltration and retention of meltwater within firn across the percolation zone of the Greenland ice sheet has the potential to buffer up to ~ 3.6 mm of global sea level rise (Harper et al., 2012). Despite evidence confirming active refreezing processes above the equilibrium line, their impact on runoff and proglacial discharge has yet to be assessed. Here we compare meteorological, melt, firn-stratigraphy and discharge data from the extreme 2010 and 2012 summers to determine the relationship between atmospheric forcing and runoff across the Kangerlussuaq catchment of the Greenland ice sheet, which drains into Watson River. The bulk discharge in 2012 of 6.8 km^3 exceeded that of 2010 of 5.3 km^3 by 28 %, despite only a 3 % difference in net energy available for melt between the two summers. This large disparity in discharge response can be explained by a 24 % contribution of runoff originating from above the long-term equilibrium line in 2012, triggered by diminished firn retention that culminated in three days of record discharge from 11 July of 3100 $m^3 s^{-1}$ (0.27 $km^3 d^{-1}$) that washed-out the Kangerlussuaq bridge.

Throughout the 2010 melt-season, there was a steady increase in the residual difference between integrated melt over the catchment and cumulative proglacial discharge that by mid-September equated to 21 % (~ 1.1 km^3) of the total melt generated being retained within the catchment. In 2012 a similar pattern is observed until 11 July, after which the residual fell by 50 % and further diminished so that less than 0.4 km^3 (~ 5 %) of the total melt was retained by the end of the summer. Cumulative energy receipts versus bulk discharge further indicate a marked contrast between the two melt-seasons, such that in 2012 there was a noteably higher discharge response per unit energy forcing after the 11 July.

Density profiles from cores and pits within the accumulation area acquired in April 2012 reveal an extensive, dense, ice-layer between 0.9 to 1.4 m snow depth that extended from the equilibrium line to at least 1840 m elevation. This perched superimposed ice layer can be attributed to melt refreezing during previous summers and

TCD
9, 4625–4660, 2015

we hypothesise that in July 2012, it provided a barrier to further infiltration rendering the underlying pore space inaccessible thereby forcing extensive runoff from the accumulation zone. Discharge was further amplified by catchment hypsometry, leading to a disproportionate increase in the area contributing to runoff as the melt-level rose above the ice sheet plateau in July 2012. Satellite imagery and oblique aerial photographs confirm an active network of supraglacial rivers extending 140 km from the ice margin providing strong support for the hypothesis.

Our findings substantiate active infiltration processes across the percolation zone of the Greenland ice sheet though the resulting patterns of refreezing are complex and can lead to spatially extensive, perched superimposed layers within the firn. In 2012, such layers extended to 1840 m providing a low-permeable obstruction to further meltwater storage, thereby promoting runoff into the hydrological system that contributed directly to sea-level rise.

1 Introduction

The Greenland ice sheet is losing mass at a rate equivalent to 0.7 mm yr^{-1} of global sea-level rise, the majority of which is attributed to surface ablation that is set to increase under atmospheric warming (Enderlin et al., 2014; Hanna et al., 2013). Although surface melt water production can be readily calculated by regional climate models (e.g. Fettweis et al., 2011) such estimates do not equate directly to sea-level rise, due to the hydrological processes that buffer and store melt on, within and beneath the ice sheet. Of these processes, it is those that determine retention near the ice sheet surface, particularly refreezing across the wet-snow/percolation zone above the equilibrium line altitude (ELA), that appear to have the greatest capacity to offset future sea-level rise (Harper et al., 2012). Within the percolation zone, melt generated at the surface infiltrates down and refreezes within the snow-pack, increasing its density, forming firn and thereby retaining potential runoff (Pfeffer et al., 1991; Braithwaite et al., 1994). An investigation by Harper et al. (2012) analysed a series of cores and

TCD
9, 4625–4660, 2015

ground penetrating radar profiles collected across an 85 km transect above the ELA at ~ 69.5° N to quantify the water storage capacity of the percolation zone. Their analysis revealed repeated infiltration events in which surface melt penetrated to more than 10 m depth and refroze as superimposed ice layers. Although the resulting patterns of vertical densification were complex, Harper et al. argue that over a period of decades such infiltration will fill up all of the available pore space thereby providing a storage sink of between 322 to 1289 Gt of melt – equivalent to buffering ~ 0.9 to ~ 3.6 mm of global sea level rise.

Below the ELA and across the ablation zone, following melt-onset in spring, melt water is initially stored within the snow-pack but once the pore-space is saturated it runs off the previous summer's ice surface (Irvine-Fynn et al., 2011). This runoff either flows directly into the subglacial environment via supraglacial river networks and moulins or is temporarily stored in supraglacial lakes. The lakes can individually capture up to 10^7 m^3 (≈ 0.01 Gt) of water (Box and Ski, 2007) and are estimated to cover up to 3 % of the ice sheet ablation area. They hence have the capacity to buffer significant volumes of water on timescales from weeks to months and if they do not drain, then potentially years (e.g. Fitzpatrick et al., 2014; Selmes et al., 2011). Once filled, the lakes contribute directly to proglacial discharge either by over-flowing into downstream moulins or by rapid in situ drainage via hydraulic fracture into the subglacial environment (e.g. Das et al., 2008; Doyle et al., 2013). It has been noted that supraglacial lakes often drain in clusters causing significant peaks in proglacial discharge (Doyle et al., 2013; Fitzpatrick et al., 2014). Ice-dammed proglacial lakes also provide a temporary buffer to proglacial discharge and are known to drain suddenly (Carrivick and Quincey, 2014; Mikkelsen et al., 2013).

Quantifying water storage mechanisms is important since the consequence of enhanced melt on the ice sheet's mass balance and contribution to global sea level depends on the fraction of melt that escapes to the ocean. The elevation of the ice sheet undergoing melt is expected to rise under predicted atmospheric warming, and this could enable runoff from well within the ice sheet interior to reach the margin and ul-

TCD
9, 4625–4660, 2015

timately contribute to enhanced sea level rise (Hanna et al., 2008; Huybrechts et al., 2011; Smith et al., 2015).

Expansion of the melt area under atmospheric warming is amplified by the ice sheet hypsometry: because the ice surface flattens toward higher elevations, a linear increase in the freezing level results in a disproportionate gain in the total surface area exposed to melt conditions. If, however, a significant fraction of that melt is subsequently intercepted by local percolation and refreezing within the snow-pack above the ELA as hypothesised by Harper et al. (2012), or otherwise at lower elevations in supraglacial lakes, then proglacial discharge and sea-level response will be buffered on a time-scale of weeks to decades. Although both of these storage terms have been estimated for the ice sheet (Box and Ski, 2007; Carrivick and Quincey, 2014; Fitzpatrick et al., 2014; Harper et al., 2012; Humphrey et al., 2012), their actual impact on runoff and proglacial discharge has yet to be assessed, primarily due to a lack of detailed measurements of proglacial discharge and surface melt runoff.

In this study, through reference to the two successive extreme-melt seasons of 2010 and 2012, we quantify the efficacy of melt storage processes through a water budget analysis. We compare surface melt with proglacial discharge across a well-defined catchment that drains the land-terminating Kangerlussuaq sector of the ice sheet. By drawing on satellite imagery and a series of snow-pits and firn-cores from above the ELA, we relate the seasonal discrepancies in the hydrological budget to the spatial extent and effectiveness of potential storage terms across the Kangerlussuaq sector of the ice sheet.

1.1 The exceptional 2010 and 2012 melt-seasons

The record warm Greenland summers of 2010 and 2012 have been studied using regional atmospheric modelling (Tedesco et al., 2013), microclimatological observations (Bennartz et al., 2013; van As et al., 2012), microwave and optical remote sensing (Nghiem et al., 2012; Smith et al., 2015; Tedesco et al., 2011), and in situ data informing an hypsometric analysis (McGrath et al., 2013). In both years, a blocking high

TCD
9, 4625–4660, 2015

pressure, associated with a strongly negative summer North Atlantic Oscillation (NAO) anomaly, was present in the mid-troposphere over Greenland (Hanna et al., 2014). The resulting circulation pattern advected warm southerly winds over the western flank of the ice sheet, forming an insulating heat-bubble over Greenland (Neff et al., 2014) that promoted enhanced surface heating.

During summer 2010, higher than average near-surface air temperatures in western and south-western regions of the ice sheet led to early and prolonged summer melting and metamorphism of surface snow, significantly reducing surface albedo and thereby enhancing sunlight absorption (Box et al., 2012; Tedesco et al., 2013; van As, 2011). Similarly, in 2012 high near-surface air temperatures and a low surface albedo enabled high melt rates. During 2012 exceptional melt events were concentrated in two periods in mid and late July. On 12 July a ridge of warm air stagnated over Greenland and melt occurred over 98.6 % of the entire surface of the ice sheet – even extending to the perennially-frozen, high-elevation interior ice at the ice divide (McGrath et al., 2013; Nghiem et al., 2012). In the Kangerlussuaq sector, the focus of this study, the 11 July 2012 melt-event had a severe and direct hazardous impact with the wash-out and partial destruction of the Watson River bridge on the 11 July 2012 (https://www.youtube.com/watch?v=RauzduvIYog and Fig. S1 in the Supplement), implying that proglacial discharge was at its highest stage since the early 1950's when the bridge was constructed. A second phase of exceptional conditions returned in late July 2012 when 79.2 % of the ice sheet surface was again exposed to melt (Nghiem et al., 2012). Bennartz et al. (2013) and Neff et al. (2014) find that low-level clouds played an important role by increasing near-surface air temperatures via their effect on radiative absorption. Such clouds were low enough to enhance the downward infrared irradiance whilst being optically thin enough to allow solar radiation to penetrate.

These conditions had the capacity to force rapid and extreme runoff from the ice sheet which emerged at the ice margin and was visible from space and in time-lapse camera sequences of, for example, proglacial flooding (Smith et al., 2015) and increased upwelling plume activity across the fronts of tidewater glaciers (Chauché

TCD
9, 4625–4660, 2015

et al., 2014; Nick et al., 2012). Nevertheless, the challenge of estimating discharge at marine-terminating glaciers, and the definitive lack of proglacial stage-gauging stations in Greenland, means that, to date, this inference can only be assessed on broad, regional scales using satellite-derived estimates of mass change (e.g. GRACE; Ewert et al., 2012).

In this study, we quantify and compare proglacial discharge and surface melt during these two years of exceptional atmospheric forcing to investigate the catchment-wide efficacy and spatio-temporal footprint of melt, storage and runoff processes across the ice sheet.

2 Study area and methods

2.1 Study area

We focus on the $\sim 10\,200\,km^2$ hydrological catchment that drains into Watson River from the land-terminating Kangerlussuaq sector on the western margin of the ice sheet. The catchment is 94 % glaciated and comprises four main outlet glaciers centred on Russell Glacier (Fig. 1). Within the catchment the ice sheet surface extends ~ 90 km from the ice margin to the mean (1990–2010) ELA of 1553 m above sea level (m a.s.l.; van de Wal et al., 2012; van de Wal et al., 2015), and on a further ~ 150 km across the accumulation area to the ice divide at ~ 2550 m a.s.l.

2.2 Proglacial discharge measurements

Proglacial river discharge was gauged at the Watson River Bridge in Kangerlussuaq, 22 to 35 km from the ice sheet margin. Due to orographic shielding by Sukkertoppen Ice Cap (Box et al., 2004; van den Broeke et al., 2008) the Kangerlussuaq region is arid, with a mean annual precipitation of 149 mm (Cappelen et al., 2001). Land surface moisture losses from evaporation minimise the land area contribution (Hasholt et al., 2013) producing negligible runoff compared to that from the inland ice area.

TCD
9, 4625–4660, 2015

Watson River discharge was determined using the stage/discharge relationship presented in Hasholt et al. (2013). Water stage was recorded by pressure transducers on a submerged rock promontory ~ 100 m upstream from the bridge, acting as a stable cross section. The discharge Q is given by

$$Q = V \times A, \quad (1)$$

where V represents the mean velocity in the river cross-section and A is the cross-sectional area. The surface velocity (V) was measured by means of a float and converted into mean cross-sectional velocity by applying a reduction factor of 0.95 (Hasholt et al., 2013). The cross-sectional area (A) used for discharge calculations is based on the deepest sounding of the channel bottom after the winter ice melts in spring. The combined uncertainty in the cross-sectional area and velocity measurements is estimated to be 15 % (Hasholt et al., 2013). However, here we also conservatively include the possibility of a systematically deeper cross section due to bed erosion within the deepest of the two channels during the runoff season. Therefore we estimate the upper limit in the yearly cumulative discharge for 2010 and 2012 at +44 % and +32 % respectively. The instantaneous possible error varies with the discharge rate, and is plotted together with the measured discharge (Fig. 2d and e).

During the flood event on 11 July 2012 the water level exceeded the previously observed maximum water stage by 1.65 m (15 %) and the stage-discharge relationship was extrapolated accordingly. Our stage-discharge relationship was also altered by the partial removal of a road dam (part of the bridge construction), which opened up two new, shallow channels between and south of the two original channels (Fig. S1). We measured the cross-sectional area of the two new channels after the flood had subsided, and by combining these measurements with estimates of the stage from time-stamped time-lapse photograph, we estimate that these new channels were 1.5 and 2.5 m deep at peak flow.

TCD
9, 4625–4660, 2015

The surface velocity in these new channels was calculated assuming the conservation of energy in fluids:

$$v = \sqrt{2gh} \tag{2}$$

where v is the surface velocity of the water, g is the gravitational acceleration ($9.82\,\mathrm{m\,s^{-2}}$) and h is the water level. The uncertainty in v for the two new channels is predominantly attributed to the determination of stage from time-lapse photos which we conservatively estimate at $\sim 30\,\%$. The two original bedrock channels remained intact and we assume that the hydraulic conditions in these channels did not change substantially during the flood event. For the period after the bridge foundation was partially washed out, the amount of discharge in the new channels is added to that calculated based on the stage/discharge relationship for the original channels. We estimate that the formation of the two new channels during the flood event resulted a low relative (i.e. $< 3\,\%$) contribution to the total discharge and they therefore do not substantially alter our results.

2.3 Meteorological measurements

Automatic weather stations (AWS) are located at three sites at elevations of 732 m a.s.l. (AWS_L), 1280 m a.s.l. (AWS_M), and 1840 m a.s.l. (AWS_U; see van As et al., 2012). Each AWS, recorded near-surface (2–3 m) air temperature, relative humidity, wind speed, air pressure, and upward and downward shortwave and long wave irradiance. Given that the temperature measured at AWS_M generally lies between that for AWS_L and U, it is omitted from Fig. 2a, but it was included in the calculations. Area-weighted positive degree-days (PDD) were calculated by interpolating the observed temperature into 100 m elevation intervals and summing the area per elevation bin.

TCD
9, 4625–4660, 2015

2.4 Snow and ice albedo

Surface albedo was determined from NASA's Terra Satellite's Moderate Resolution Imaging Spectroradiometer (MODIS) interpolated onto a 5 km grid from 1 May 2010 to 31 September 2012. A 11 day running median was taken to reject occasional noise (e.g. caused by contrails) from the time series (Box et al., 2012). From these data an albedo time series was formed for the glaciated part of the Watson River catchment area defined as $67 \pm 0.2^{\circ}$ N, and west of 44° W. The data were averaged in 100 m elevation intervals. The data were further generalised by three elevation bands which equate to the extent of the dark-, lake- and wet-snow zones, respectively (Fig. 1).

2.5 Surface energy budget model

The surface energy budget (SEB) was calculated at a daily time step following (van As, 2011). The model calculates radiative, turbulent, rain and subsurface (conductive) energy fluxes using the AWS measurements as input, interpolated into the same 100 m elevation bins as the albedo data. The MODIS albedo data were assimilated to improve the elevation-binned calculation of net shortwave radiation. The sensible and latent heat fluxes were calculated from near surface gradients of wind speed, temperature and humidity using a stability correction. The surface mass balance (SMB) is calculated as the sum of solid precipitation, surface melt and sublimation. The model was subsequently validated against independent K-transect measurements (e.g. van de Wal et al., 2005, 2012) and modelled ablation was within 4 % of the observed values. Importantly; to determine exactly what melt was available as runoff each year, and quantify the specific proportion of total melt integrated across the catchment that contributed to proglacial discharge or otherwise was retained, the parameterisation that calculates refreezing and water retention of water in snow/firn was disabled for this study.

TCD
9, 4625–4660, 2015

2.6 Supraglacial lake drainage

To determine the extent and timing of supraglacial lake drainage events within the Watson River catchment, an automatic lake classification was applied to daily MODIS MOD09 imagery following the methodology of Fitzpatrick et al. (2014). Fifty-two cloud-free, atmospherically corrected images were processed to derive the surface area and volume of supraglacial lakes. Lake areas are classified using an empirically-determined threshold of the Normalised Difference Water Index (NDWI; Huggell et al., 2002). Lake volume is derived using a reflective index approach (Box and Ski, 2007) calibrated against lake bathymetry data that was acquired in 2010 (Doyle et al., 2013), and subsequently validated against independently-derived depths from a supraglacial lake at 67° N, 48° W, at ~ 1420 m.a.s.l. (Fitzpatrick et al., 2014). The uncertainty in lake area and depth is estimated at $\pm 0.2\,km^2$ per lake and 1.5 m per pixel respectively. Change in stored volume in each lake was converted to mean discharge rates between cloud-free observations (Fig. 2d and e).

2.7 Catchment delineation

A well documented source of uncertainty in estimating runoff from distributed melt modelling stems from the delineation of the glaciated watershed (e.g. van As et al., 2012; Fitzpatrick et al., 2014; Smith et al., 2015). In this study we use a modified version of the catchment based on Hasholt et al. (2013), modified by Fitzpatrick et al. (2014) from the delineation of surface topography combined with the mapping of supraglacial hydrological features (Fig. 1a and d). Fitzpatrick et al. (2014) compare the numerous watersheds published and verify the reliability of the optimum catchment delineation (used here) by comparison against multiple Landsat imagery to ensure that no supraglacial streams crossed the watersheds during the melt-season; a method used effectively in the neighboring Isortoq catchment by Smith et al. (2015). By following the stream and river networks from their start to their terminus either in melt lakes or moulins, it is assured that the delineated watershed encompassed the complete supraglacial

TCD
9, 4625–4660, 2015

network that contributed to Watson River catchment and proglacial discharge. Transient migration and water piracy between catchments is possible, likely even, given that catchment boundaries will change depending on the state of both the supraglacial and subglacial hydrological systems (Lindbäck et al., 2015). Greatest uncertainty in watershed geometry and delineation is though most apparent in the upper catchment where the ice surface is flattest but is mitigated by reduced melt at high elevations. Currently the available data for the subglacial topography is insufficient to make accurate subglacial catchment predictions and we therefore use the surface derived watershed as per previous studies.

2.8 Measurements of firn and snow pack density

To investigate firn and snow-pack densification, 15 snow-pits and three shallow ice cores were obtained from eight sites between 1280 and 1840 m a.s.l. in April 2012. Two cores (#1 and #2) were drilled 10 m apart in the direct vicinity of AWS_U while core #3 was drilled at a site located 400 m to the south of AWS_U. The stratigraphy and density of the snow and firn was studied in these 7.6 cm diameter cores to a depth of 10 m. The core stratigraphy was analysed visually at ~ 1 cm vertical resolution before cores were cut into 10 cm sections and weighed to determine the density profile of the snowpack and firn. A transect of 0.5 to 1 m deep snow-pits between AWS_M and AWS_U were examined to investigate spatial variations in firn and snowpack density (Fig. 1).

3 Results

Near-surface air temperatures from three AWS indicate differences in the temporal and altitudinal distribution of heating in 2010 and 2012. Melt commenced earlier in 2010 with the lowest AWS_L reaching 6 °C daily average air temperature by mid-May (Fig. 2a). At AWS_L, melt with air temperature 5 °C above the seasonal average persisted until 15 September. The duration of the 2010 melt-season (119 days) was with-

TCD
9, 4625–4660, 2015

out precedent for this sector of the ice sheet since instrument records began in Kangerlussuaq (van As et al., 2012). At the uppermost AWS_U, ~ 300 m above the 1991–2009 baseline ELA of 1524 m (van de Wal et al., 2012), above-freezing temperatures did not prevail until 8 July 2010. Thereafter daily temperatures remained generally elevated until September making 2010 exceptional compared to the long-term mean, particularly at high elevations.

In contrast, during 2012 air temperatures at elevations above the mean ELA were above freezing from mid-June onwards and included two week-long periods with daily air temperatures at AWS_U of 3 to 4 °C (Fig. 2a), coinciding with persistent anomalously high barometric pressure and associated clear sky conditions. During the 5 day period leading up to the extreme mid-July 2012 melt event, air temperatures at AWS_M and AWS_U were similar, despite over 70 km horizontal and 500 m vertical separation. Hence, from mid June and throughout July 2012, the environmental lapse rate was near zero – indicating that melting conditions prevailed across a large portion of the gently sloping accumulation area. By the 12 July, melt extended across the entire accumulation area to the topographic peak of the ice sheet (McGrath et al., 2013; Nghiem et al., 2012). At lower elevations, the mean 2012 summer air temperatures were 0.75 °C lower than in 2010, although they were still higher than the long-term mean, explained, in part, by the delayed 2012 melt onset, commencing in late May 2012 (Fig. 2a).

The physical expression of atmospheric forcing in terms of energy available for surface melt can be represented by area-weighted cumulative positive degree-days (ΣPDD'). ΣPDD' had nearly equivalent totals by the end of the 2010 and 2012 melt-seasons with 2012 just 5 % higher (Fig. 2b, Table 1). The difference can be, at least partially, explained by both the earlier 2010 melt onset and the higher peak 2012 warm-episodes, compared to the 2010 peak which occurred in August. By 1 July 2012, ΣPDD' exceeded that of 2010, revealing that greater energy was available for melting throughout this month. In August 2010, ΣPDD' was boosted by the sustained warm-episode across the entire catchment, particularly at higher elevations – as recorded by AWS_U. The 2010 warm episode persisted until September and by the end of the melt-seasons

TCD
9, 4625–4660, 2015

in 2010 and 2012 the catchment received nearly equivalent total net inputs of energy from the atmosphere to drive surface melt. For comparison, the total energy available for melt in 2010 and 2012 calculated using the SEB model for the catchment up to an elevation of 1840 m a.s.l. was only 3 % larger in 2012, compared to 2010 (Table 1). MODIS derived albedo time-series (Fig. 2c) are split into three approximately equal-area, elevation bands corresponding to the physiographic regions of impurity darkness (1000 to 1450 m a.s.l., lakes (1500–1650 m a.s.l.) and wet-snow (1700–1850 m a.s.l.; Fig. 1; Wientjes et al., 2010, 2012; Wientjes and Oerlemans, 2010). In early summer, albedo patterns for 2010 and 2012 were similar until mid-June. In 2012, the albedo decline lags behind that of 2010 due to the early-May melt onset in 2010, which was compounded by low 2009/2010 winter snow accumulation (van As et al., 2012). By mid-June, albedo across the dark zone for both years declined to 0.4. For the remainder of the season, the 2010 dark zone albedo was ∼ 0.05 lower than in 2012 (Fig. 2c), which is likely owing to the warmer temperatures and enhanced melt at low elevations during the 2010 melt season. Across the lake and wet-snow zones, a similar pattern of albedo decline is observed up until mid-June. From this time onwards, in contrast to the dark zone, it is 2012 albedo that is consistently and as much as 0.2 lower than 2010, with the exception of a week-long, snow-fall albedo reset on 5 August 2012. Enhanced black carbon deposition from North American wildfire is likely to have played a key role in driving the exceptionally low albedo at high elevations in 2012 (Keegan et al., 2014).

Daily Watson River discharge and catchment-integrated melt differed considerably between 2010 and 2012 (Fig. 2d, e, f). In 2010 the integrated melt and discharge gradually increased at a slower rate than during 2012, despite higher cumulative PDD and lower albedo. 2012 measured discharge reached 3100 $m^3 s^{-1}$ (equivalent to ∼ 0.27 $km^3 d^{-1}$; Fig. 3e) in mid-July, and which partially destroyed Watson River bridge (Fig. S1). With lower temperatures during the week commencing the 15 July, melt and discharge dropped to below 2010 levels but returned to high values (∼ 1500 $m^3 s^{-1}$) for 11 days starting on 26 July 2012, coincident with the second phase of exceptionally

TCD
9, 4625–4660, 2015

warm conditions. The annual total measured discharge in 2012 of 6.8 km^3 −15/+32 % exceeded the 2010 total of 5.3 km^3 by ∼ 28 %.

Throughout the 2010 melt-season, there was a steady increase in the residual between calculated melt across the catchment and cumulative proglacial discharge, which by the end of the season equated to 21 % (∼ 1.1 km^3) of residual melt retained (R') within the catchment (Fig. 2f). In the period leading up to 11 July 2012 a similar R' as compared to 2010 suggests meltwater storage. After 11 July 2012 however, R' drops by 50 % and reduces further by the end of the season indicating that < 0.2 km^3 of meltwater is retained in the catchment, and that meltwater retention after 11 July 2012 was limited. The plot of cumulative energy input vs. cumulative discharge in 2010 and 2012 (Fig. 3) demonstrates that the catchment responds differently to the varying energy input in the two years. The slope of the cumulative measured discharge vs. cumulative calculated energy input is steeper in 2012 than in 2010; meaning that for a given energy input, there was a higher discharge response in 2012 compared to 2010. Especially during the flooding period (11 to 14 July 2012) the curve diverges in slope, where the discharge response to the energy input is stronger, i.e. a steeper slope.

Table 2 lists calculated melt totals from different elevation intervals with Watson River discharge totals and their differences. Below the mean ELA, the two years are almost equal in terms of calculated melt (5 % difference). By contrast, above the ELA at elevations up to 1840 m a.s.l. and 2050 m, the melt was 106 and 231 % greater respectively in 2012 compared to 2010. Despite this, the difference in total calculated melt between the two years, was still no more than 4 and 9 % for the totals, depending on the elevation to which melt is included. Yet the difference in measured proglacial discharge between the two years peaks at 28 %. Thus the runoff response to energy input and atmospheric forcing was higher in 2012, reflected in the residual between calculated melt and measured proglacial discharge (Fig. 2f) and the illustration of discharge response to energy input (Fig. 3).

The timing of integrated melt and Watson River discharge (Fig. 2d and e) in both years demonstrates that meltwater routing through the glacial and proglacial system

TCD
9, 4625–4660, 2015

is efficient with a delay of between 1 to 5 days throughout each melt-season. In June 2012, the proglacial discharge response to melt was dampened and delayed. Through July and the beginning of August 2012, the proglacial discharge responds to melt production with a shorter lag. Prior to the 11 July 2012 extreme melt and discharge, the integrated modelled melt closely resembles the proglacial discharge hydrograph but with a ~ 3 day lag. The implication is that once local meltwater production had been mobilised, even at high elevations within the percolation area, the runoff transits within 3 days through a drainage network up to 160 km distant from the gauging station, and contributes to the proglacial discharge peak. Under these conditions, supra- and sub-glacial routing can be termed "efficient" on comparison to those transit times derived from tracers up to 57 km from the ice margin in 2011 (Chandler et al., 2013), with derived mean velocity exceeding 2 km h^{-1} (~ 0.6 m s^{-1}). The second phase of intense melt starting 26 July 2012 resulted in a rapid rise in discharge with a lag of just ~ 2 days. Peak melt during this period occurred on 3 August with the peak in proglacial discharge on the 5 August occurring before rapid abatement concurrent with declining air temperatures from the 6 August onwards.

Water stored and released from supraglacial lakes accounted for a minor component of proglacial discharge. Further, in 2010 and 2012 the majority of lake drainages occurred before any peaks in proglacial discharge (Fig. 2e and f). The calculated mean drainage rate of < 100 m^3 s^{-1} for 2012 clearly indicates that the volume of lake drainage water contributed less than 2 % of the total bulk discharge (Fig. 2d and e). The maximum short-term contribution from lake drainage (0.10 km^3) occurred on 23 June 2012 with the drainage of a cluster of five lakes (Fig. 2e). Over the following week, approximately 70 % of all the water stored in supraglacial lakes across the catchment was released (Fig. 2e), which potentially accounts for as much as half of the discharge. However, this widespread lake drainage was ~ 12 days before the extreme proglacial discharge event of 11 July 2012. Supraglacial lakes can empty in as little as 2 h (Das et al., 2008; Doyle et al., 2013) and it is likely that the lake water exited the glacial

TCD
9, 4625–4660, 2015

system before 11 July. One ~ 0.02 km^3 lake drainage between 5 and 8 July could have contributed ~ 2 % to the record discharge between 10 and 14 July (0.9 km^3).

MODIS and Landsat imagery reveal that no proglacial ice-dammed lakes within the catchment drained prior to the flooding event, including a number that appear to drain regularly in August/September each year (Mikkelsen et al., 2013). On 11 September 2010 and 12 August 2012, a number of proglacial lakes did drain, though their net contribution to the proglacial discharge was insignificant (Fig. 2d and e).

4 Discussion

Despite the cumulative PDD sum and calculated energy available for melt being only 5 and 3 %, respectively larger in 2012 than in 2010 (Table 1), the measured proglacial discharge response was 28 % greater in 2012 compared to 2010 (Fig. 2f and Table 2). The total energy inputs for 2010 and 2012 were very similar (Fig. 3) but the ensuing runoff responses were remarkably different (Fig. 3). Widespread melt in 2010 has been ascribed to atmospherically-sourced heating coupled with the albedo feedback that was promoted by low winter snowfall and early melt onset (Box et al., 2012; Tedesco et al., 2011; van As et al., 2012). Yet low albedo and high air temperatures alone cannot explain the 28 % increase in discharge in 2012 compared to 2010. Analysis of MODIS imagery confirms that the release of stored water from supraglacial lakes played a relatively minor role in the peak and total proglacial hydrograph in 2012 (Fig. 2d and e). At most, the supraglacial lake contribution to the 11 July 2012 peak discharge of 3100 $m\,s^{-1}$ was < 2 %. We have no information on the relative importance of englacial and subglacial storage/release of which there is likely to be some component (Rennermalm et al., 2013). However, during our investigation period or historically there is no incidence of large discharge independent of extreme discharge events, except from jökulhlaups originating from ice-dammed lakes located at the ice-margin (Mikkelsen et al., 2013; Russell, 2011). Our results indicate that only a relatively small amount of the total melt generated is stored in supraglacial lakes and that the buffering effect of

TCD
9, 4625–4660, 2015

lakes on runoff is hence limited (Fig. 2d and e). That is not to completely dismiss the role of lakes in ice sheet hydrology, since once a lake drains it henceforth provides an efficient englacial pathway via moulins for surface melt to directly access the subglacial environment for the remainder of the melt season (e.g. Das et al., 2008; Doyle et al., 2013).

We invoke three compatible explanations for the exceptional discharge observed in 2012: (1) significant melt occurring both below and above ELA; (2) ice surface hypsometry (the flattening of the ice sheet towards high elevations) amplified the total melt and potential runoff generated above the ELA by disproportionately increasing the contributing area when melt reached into the accumulation area (Fig. 1b and c); and (3) limited firn-retention and storage capacity in the accumulation area promoting large scale runoff from this high elevation area. It is important that runoff from above the mean ELA, and particularly from the percolation area can only be accommodated if firn-retention capacity was severely reduced in 2012, which herein forms the central hypothesis of our discussion. We thus present three additional lines of evidence: (a) Snow pit observations and ice core straigraphy acquired in April 2012; (b) observations of surface water obtained from satellite imagery and field observations in the vicinity of AWS_U (Fig. 5); and (c) results of a SEB modelling experiment where total integrated melt is assumed to runoff without any retention or refreezing.

Logged stratigraphy in May 2012 for all three firn-cores was broadly similar, with the following main characteristics: winter snow down to 0.55 or 0.70 m (the surface snow layer was discarded in cores #1 and #2 and instead measured in a nearby snow pit), coarse grained firn below the winter snow, a first pronounced ice layer (5 cm) at 115 cm depth, and a massive 0.3 to 0.5 m thick ice layer commencing at a depth of 1.55 to 1.70 m. Beneath this ice layer to 2.5 m depth, snow, ice and firn layers alternate. The measured density profiles (Fig. 4a–c.) confirm this observed stratigraphy. A persistent decimetre-thick layer of ice formed from refrozen melt was observed in 15 snow pits dug along a transect from 1500 m to AWS_U (Figs. 1 and 5). Reduced firn-retention due to a superimposed, perched ice lens is further supported by energy balance modelling of

TCD
9, 4625–4660, 2015

the near-surface water table at AWS_U (Fig. 4d). Here two potential sets of blocking-lenses at different levels within the snow-pack equate to the thick superimposed ice lenses observed in the firn cores acquired (Fig. 4a–c). For the shallowest of these scenarios, melt and retention calculations predict complete saturation and free surficial water available for runoff by 11 July.

Evidence for firn saturation and flowing surface water are obtained from the identification of an active supraglacial channel network in Landsat satellite imagery and observations in the vicinity of AWS_U (Fig. 5). Wet snow, meltwater channels and lakes can be identified up to at least 1750 m a.s.l. from 23 June 2012, and an active stream network up to 1800 m a.s.l. from mid-July 2012 onwards. In early August 2012 field observation of an active channel network were confirmed during an annual maintenance visit to AWS_U (Fig. 5b and c). These observed supraglacial hydrological features above the long-term ELA in the period leading up to the 2012 peak discharge event support the snow-pack modelling and provide the first unequivocal evidence for complete saturation of the surface layer at AWS_U by mid-July 2012. They also demonstrate that melt-retention by firn at elevations at least to ~ 300 m above and ~ 60 km from the ELA in this sector of the ice sheet played a minimal role in buffering runoff in July 2012.

If predicted future climate warming is realised, the combined effect of reduced firn retention capacity and ice sheet hypsometry will become increasingly important in amplifying the runoff response to melt. If, as we hypothesise, the extraordinary discharge in 2012 was substantially derived from runoff from above the ELA and up to 1840 m a.s.l. driven by a low permeable, superimposed ice lens formed during previous warm summers, then the extensive melt that accompanied the July 2012 warming would likely lead to the formation of even thicker, superimposed ice layers extending further into the accumulation area. We envisage a similar, amplified runoff response to future atmospherically forced melt events that will lead to further dramatic proglacial discharge rates as observed in 2012. Under these conditions, the firn-buffering mechanism inferred for the EGIG line, located 120 km north of our study area, by Harper et al. (2012),

TCD
9, 4625–4660, 2015

and which was extrapolated across the entire ice sheet, would appear to be much diminished, at least in the Kangerlussuaq sector. Analysis of their data (Figs. 2b and 3c of Harper et al., 2012) from the equivalent location, indicates that our AWS_U site, located 50 km inland from, and 300 m above the ELA, should have had a buffering capacity of ∼ 60 %, which equates to a fill-depth of at least 2 m and potentially up to 10 m of water equivalent melt. Clearly, in 2012 this was not the case and melt was forced to runoff into an active supraglacial hydrological network thereby directly contributing to proglacial discharge and sea-level rise.

5 Conclusions

The extraordinary discharge of $\sim 3100\,m^3\,s^{-1}$ observed between 11 and 14 July 2012 provides a natural experiment to assess of the ice sheet response to an extreme episode of atmospheric forcing, and furthermore, allows us to resolve and attribute the source of that runoff. The bulk discharge of $6.8\,km^3$ measured in Watson River in 2012 was unprecedented since the Kangerlussuaq bridge was constructed in the early 1950's and exceeded the previous record set in 2010 by ∼ 28 %. Throughout the 2010 melt-season, there was a steady increase in the residual between calculated melt across the catchment and cumulative proglacial discharge, which by the end of the season equated to 21 % (∼ $1.1\,km^3$) melt retained within the catchment. In the period leading up to 11 July 2012 a similar pattern indicates significant meltwater storage. In contrast, in 2012 after 11 July the residual fell by 50 % and reduced further by the end of September revealing that less than $0.4\,km^3$ of meltwater was retained in the catchment. Cumulative energy input vs. cumulative discharge in 2010 and 2012 demonstrates that the catchment experienced a marked transition in response to atmospheric energy forcing in the two years. The slope of the cumulative measured discharge vs. cumulative calculated energy input is steeper in 2012 than in 2010; meaning that for a given energy input, there was a higher discharge response in 2012 compared to 2010, particularly during the 11 July flood. We infer that in 2010 melt from elevations above the ELA

TCD
9, 4625–4660, 2015

was buffered by percolation and refreezing within firn. In contrast, after 11 July 2012, we find evidence from observations and modelling that firn-layer retention and buffering above the ELA to at least 1840 m a.s.l. was much reduced by an extensive perched, thick and low permeable ice lens – very likely formed in previous, record (e.g. 2007 and 2010) melt years. Hence, the firn-buffering mechanisms observed on the EGIG line and extrapolated across the ice sheet by Harper et al. (2012) appear to be severely limited – at least in the Kangerlussuaq sector of the ice sheet – in 2012.

The next decade will reveal if 2010 and 2012 were exceptionally rare melt seasons due to natural variability or are an emerging pattern of new extreme high melt years. In either case, it is critical to understand the runoff response of the ice sheet to such events to determine what portion of the melt generated is intercepted and stored on the ice sheet and what fraction directly contributes to proglacial discharge and sea-level rise.

Our results reveal that such firn-retention and buffering effects were much reduced in 2012, and hence there was a near-instantaneous discharge response, with a disproportionately larger area of the upper ice sheet surface contributing to runoff and thereby contributing directly to global sea level rise.

The Supplement related to this article is available online at doi:10.5194/tcd-9-4625-2015-supplement.

Acknowledgements. We thank Dirk van As and Horst Machguth for valuable inputs during the preparations of the manuscript. Gratitude also goes to Paul Smeets, Institute for Marine and Atmospheric Research, Utrecht University for providing oblique areal pictures taken at AWS_U on 13 August 2012. We acknowledge support from the Greenland Analogue Project (GAP), the commission on scientific investigations in Greenland, grant no. 07-015998, 09-064628 and 2138-08-0003 and the Danish National Research Foundation founding Centre for Permafrost (CENPERM), funded by the Danish National Research Foundation, DNRF number 100, Department of Geosciences and Nature Resource Management, University of Copenhagen, Denmark for financial support of the discharge measurements. The on-ice weather stations in this

TCD
9, 4625–4660, 2015

study were installed and maintained by GEUS and Aberystwyth University through GAP and UK NERC funding. J. Box is here supported by Denmark's "Det Frie Forskningsråd", Nature og Universe grant DFF – 4002-00234. The National Aeronautics and Space Administration (NASA) award NNX10AR76G provided funding for the firn table modelling work through the Cooperative Institute for Research in Environmental Sciences, University of Colorado at Boulder, USA. A. Fitzpatrick and S. Doyle were supported by Aberystwyth University Research Studentships and fieldwork was supported by NERC Projects NE/G005796/1, NE/G010595/1, NE/H024204/1 and a Royal Geographical Society Gilchrist Fieldwork Award. A. Hubbard kindly acknowledges support from the Centre for Arctic Gas Hydrate, Environment and Climate by funding from the Research Council of Norway (Grant No. 223259).

References

Bennartz, R., Shupe, M. D., Turner, D. D., Walden, V. P., Steffen, K., Cox, C. J., Kulie, M. S., Miller, N. B., and Pettersen, C.: July 2012 Greenland melt extent enhanced by low-level liquid clouds, Nature, 496, 83–86, 2013.

Box, J. E. and Ski, K.: Remote sounding of Greenland supraglacial melt lakes: implications for subglacial hydraulics, J. Glaciol., 53, 257–265, 2007.

Box, J. E., Bromwich, D. H., and Bai, L.-S.: Greenland ice sheet surface mass balance 1991–2000: application of Polar MM5 mesoscale model and in situ data, J. Geophys. Res., 109, D16105, doi:10.1029/2003JD004451, 2004.

Box, J. E., Fettweis, X., Stroeve, J. C., Tedesco, M., Hall, D. K., and Steffen, K.: Greenland ice sheet albedo feedback: thermodynamics and atmospheric drivers, The Cryosphere, 6, 821–839, doi:10.5194/tc-6-821-2012, 2012.

Braithwaite, R. J., Laternser, M., and Pfeffer, T.: Variations of near-surface firn density in the lower accumulation area of the Greenland ice sheet, Pakitsoq, West Greenland, J. Glaciol., 40, 477–485, 1994.

Cappelen, J., Jørgensen, B. V., Laursen, E. V., Stannius, L. S., and Thomsen, R. S.: Technical Report 00-18: The observed climate of Greenland, 1958–99 – with climatological standard normals, 1961–90, Danish Meteorological Institute, Copenhagen, 2001.

TCD
9, 4625–4660, 2015

Carrivick, J. L. and Quincey, D. J.: Progressive increase in number and volume of ice-marginal lakes on the western margin of the Greenland Ice Sheet, Global Planet. Change, 116, 156–163, 2014.

Chandler, D. M., Wadham, J. L., Lis, G. P., Cowton, T., Sole, A., Bartholomew, I., Telling, J., Nienow, P., Bagshaw, E. B., Mair, D., Vinen, S., and Hubbard, A.: Evolution of the subglacial drainage system beneath the Greenland Ice Sheet revealed by tracers, Nat. Geosci., 6, 195–198, 2013.

Chauché, N., Hubbard, A., Gascard, J.-C., Box, J. E., Bates, R., Koppes, M., Sole, A., Christoffersen, P., and Patton, H.: Ice–ocean interaction and calving front morphology at two west Greenland tidewater outlet glaciers, The Cryosphere, 8, 1457–1468, doi:10.5194/tc-8-1457-2014, 2014.

Das, S. B., Joughin, I., Behn, M. D., Howat, I. M., King, M. A., Lizarralde, D., and Bhatia, M. P.: Fracture propagation to the base of the Greenland Ice Sheet during supraglacial lake drainage, Science, 320, 778–781, 2008.

Doyle, S. H., Hubbard, A. L., Dow, C. F., Jones, G. A., Fitzpatrick, A., Gusmeroli, A., Kulessa, B., Lindback, K., Pettersson, R., and Box, J. E.: Ice tectonic deformation during the rapid in situ drainage of a supraglacial lake on the Greenland Ice Sheet, The Cryosphere, 7, 129–140, doi:10.5194/tc-7-129-2013, 2013.

Enderlin, E. M., Howat, I. M., Jeong, S., Noh, M. J., van Angelen, J. H., and van den Broeke, M. R.: An improved mass budget for the Greenland ice sheet, Geophys. Res. Lett., 41, 866–872, 2014.

Ewert, H., Groh, A., and Dietrich, R.: Volume and mass changes of the Greenland ice sheet inferred from ICESat and GRACE, J. Geodyn., 59–60, 111–123, 2012.

Fettweis, X., Belleflamme, A., Erpicum, M., Franco, B., and Nicolay, S.: Estimation of the sea level rise by 2100 resulting from changes in the surface mass balance of the Greenland Ice Sheet, in: Climate Change: Geophysical Foundations and Ecological Effects, edited by: Blanco, J. and Kheradmand, H., InTech, Croatia ,2011.

Fitzpatrick, A. A. W., Hubbard, A. L., Box, J. E., Quincey, D. J., van As, D., Mikkelsen, A. P. B., Doyle, S. H., Dow, C. F., Hasholt, B., and Jones, G. A.: A decade (2002–2012) of supraglacial lake volume estimates across Russell Glacier, West Greenland, The Cryosphere, 8, 107–121, doi:10.5194/tc-8-107-2014, 2014.

TCD
9, 4625–4660, 2015

Hanna, E., Huybrechts, P., Steffen, K., Cappelen, J., Huff, R., Shuman, C., Irvine-Fynn, T., Wise, S., and Griffiths, M.: Increased runoff from melt from the Greenland ice sheet: a response to global warming, J. Climate, 21, 331–341, 2008.

Hanna, E., Navarro, F. J., Pattyn, F., Domingues, C. M., Fettweis, X., Ivins, E. R., Nicholls, R. J., Ritz, C., Smith, B., and Tulaczyk, S.: Ice-sheet mass balance and climate change, Nature, 498, 51–59, 2013.

Hanna, E., Fettweis, X., Mernild, S. H., Cappelen, J., Ribergaard, M. H., Shuman, C. A., Steffen, K., Wood, L., and Mote, T. L.: Atmospheric and oceanic climate forcing of the exceptional Greenland ice sheet surface melt in summer 2012, Int. J. Climatol., 34, 1022–1037, 2014.

Harper, J., Humphrey, N., Pfeffer, W. T., Brown, J., and Fettweis, X.: Greenland ice-sheet contribution to sea-level rise buffered by meltwater storage in firn, Nature, 491, 240–243, 2012.

Hasholt, B., Mikkelsen, A. B., Nielsen, M. H., and Larsen, M. A. D.: Observations of runoff and sediment and dissolved loads from the Greenland ice sheet at Kangerlussuaq, West Greenland, 2007 to 2010, Z. Geomorphol., 57, 3–27, 2013.

Huggell, C., Kaab, A., Haeberli, W., Teysseire, P., and Paul, F.: Remote sensing based assessment of hazards from glacier lake outbursts: a case study in the Swiss Alps, Can. Geotech. J., 39, 316–330, 2002.

Humphrey, N. F., Harper, J. T., and Pfeffer, W. T.: Thermal tracking of meltwater retention in Greenland's accumulation area, J. Geophys. Res.-Earth, 117, F01010, doi:10.1029/2011JF002083, 2012.

Huybrechts, P., Goelzer, H., Janssens, I., Driesschaert, E., Fichefet, T., Goosse, H., and Loutre, M. F.: Response of the Greenland and Antarctic ice sheets to multi-millennial greenhouse warming in the earth system model of intermediate complexity LOVECLIM, Surv. Geophys., 32, 397–416, 2011.

Irvine-Fynn, T. D. L., Hodson, A. J., Moorman, B. J., Vatne, G., and Hubbard, A. L.: Polythermal glacier hydrology: a review, Rev. Geophys., 49, RG4002, doi:10.1029/2010RG000350, 2011.

Keegan, K. M., Albert, M. R., McConnell, J. R., and Baker, I.: Climate change and forest fires synergistically drive widespread melt events of the Greenland Ice Sheet, P. Natl. Acad. Sci. USA, 111, 7964–7967, 2014.

Lindbäck, K., Pettersson, R., Hubbard, A., L., Doyle S., H., van As, D., Mikkelsen, A. B., and Fitzpatrick, A. A.: Subglacial water drainage and piracy beneath the Greenland Ice Sheet, Geophys. Res. Lett., L065393, accepted, 2015.

TCD
9, 4625–4660, 2015

McGrath, D., Colgan, W., Bayou, N., Atsuhiro, M., and Konrad, S.: Recent warming at Summit, Greenland: Global contect and implications, Geophys. Res. Lett., 40, 2091–2096, 2013.
Mikkelsen, A. B., Hasholt, B., Knudsen, N. T., and Nielsen, K.: Jökulhlaups and sediment transport in Watson River, Kangerlussuaq, West Greenland, Hydrol. Res., 44, 58–67, 2013.
Neff, W., Compo, G. P., Ralph, F. M., and Shupe, M. D.: Continental heat anomalies and the extreme melting of the Greenland ice surface in 2012 and 1889, J. Geophys. Res.-Atmos., 119, 6520–6536, 2014.
Nghiem, S. V., Hall, D. K., Mote, T. L., Tedesco, M., Albert, M. R., Keegan, K., Shuman, C. A., DiGirolamo, N. E., and Neumann, G.: The extreme melt across the Greenland ice sheet in 2012, Geophys. Res. Lett., 39, L20502, doi:10.1029/2012GL053611, 2012.
Nick, F. M., Luckman, A., Vieli, A., van der Veen, C. J., van As, D., van de Wal, R. S. W., Pattyn, F., Hubbard, A. L., and Floricioiu, D.: The response of Petermann Glacier, Greenland, to large calving events, and its future stability in the context of atmospheric and oceanic warming, J. Glaciol., 58, 229–239, 2012.
Pfeffer, W. T., Meier, M. F., and Illangasekare, T. H.: Retention of Greenland runoff by refreezing – Implications for projected future sea-level change, J. Geophys. Res.-Oceans, 96, 22117–22124, 1991.
Rennermalm, A., Moustafa, S., Mioduszewski, J., Chu, V., Forster, R., Hagedorn, B., Harper, J., Mote, T., Robinson, D., Shuman, C., Smith, L. C. and Tedesco, M.: Understanding Greenland ice sheet hydrology using an integrated multi-scale approach, Environ. Res. Lett., 8, 015017, doi:10.1088/1748-9326/8/1/015017, 2013.
Russell, A. J., Carrivick, J. L., Ingeman-Nielsen, T., Yde, J. C., and Williams, M.: A new cycle of jokulhlaups at Russell Glacier, Kangerlussuaq, West Greenland, J. Glaciol., 57, 238–246, 2011.
Selmes, N., Murray, T., and James, T. D.: Fast draining lakes on the Greenland Ice Sheet, Geophys. Res. Lett., 38, L15501, doi:10.3189/002214311796405997, 2011.
Smith, L. C., Chu, V. W., Yang, K., Gleason, C. J., Pitcher, L. H., Rennermalm, A. K., Legleiter, C. J., Behar, A. E., Overstreet, B. T., Moustafa, S. E., Tedesco, M., Forster, R. R., LeWinter, A. L., Finnegan, D. C., Sheng, Y., and Balog, J.: Efficient meltwater drainage through supraglacial streams and rivers on the southwest Greenland ice sheet, P. Natl. Acad. Sci. USA, 112, 1001–1006, 2015.

TCD
9, 4625–4660, 2015

Tedesco, M., Fettweis, X., van den Broeke, M. R., van de Wal, R. S. W., Smeets, C. J. P. P., van de Berg, W. J., Serreze, M. C., and Box, J. E.: The role of albedo and accumulation in the 2010 melting record in Greenland, Environ. Res. Lett., 6, 1–6, 2011.

Tedesco, M., Fettweis, X., Mote, T., Wahr, J., Alexander, P., Box, J. E., and Wouters, B.: Evidence and analysis of 2012 Greenland records from spaceborne observations, a regional climate model and reanalysis data, The Cryosphere, 7, 615–630, doi:10.5194/tc-7-615-2013, 2013.

van As, D.: Warming, glacier melt and surface energy budget from weather station observations in the Melville Bay region of northwest Greenland, J. Glaciol., 57, 208–220, 2011.

van As, D., Hubbard, A. L., Hasholt, B., Mikkelsen, A. B., van den Broeke, M. R., and Fausto, R. S.: Large surface meltwater discharge from the Kangerlussuaq sector of the Greenland ice sheet during the record-warm year 2010 explained by detailed energy balance observations, The Cryosphere, 6, 199–209, doi:10.5194/tc-6-199-2012, 2012.

van de Wal, R. S. W., Greuell, W., van den Broeke, M. R., Reijmer, C. H., and Oerlemans, J.: Surface mass-balance observations and automatic weather station data along a transect near Kangerlussuaq, West Greenland, Ann. Glaciol., 42, 311–316, 2005.

van de Wal, R. S. W., Boot, W., Smeets, C. J. P. P., Snellen, H., van den Broeke, M. R., and Oerlemans, J.: Twenty-one years of mass balance observations along the K-transect, West Greenland, Earth Syst. Sci. Data, 4, 31–35, doi:10.5194/essd-4-31-2012, 2012.

van de Wal, R. S. W., Smeets, C. J. P. P., Boot, W., Stoffelen, M., van Kampen, R., Doyle, S. H., Wilhelms, F., van den Broeke, M. R., Reijmer, C. H., Oerlemans, J., and Hubbard, A.: Self-regulation of ice flow varies across the ablation area in south-west Greenland, The Cryosphere, 9, 603–611, doi:10.5194/tc-9-603-2015, 2015.

van den Broeke, M., Smeets, P., Ettema, J., and Munneke, P. K.: Surface radiation balance in the ablation zone of the west Greenland ice sheet, J. Geophys. Res., 113, D13105, doi:10.1029/2007JD009283, 2008.

Wientjes, I. G. M. and Oerlemans, J.: An explanation for the dark region in the western melt zone of the Greenland ice sheet, The Cryosphere, 4, 261–268, doi:10.5194/tc-4-261-2010, 2010.

Wientjes, I. G. M., Van de Wal, R. S. W., Reichart, G. J., Sluijs, A., and Oerlemans, J.: Dust from the dark region in the western ablation zone of the Greenland ice sheet, The Cryosphere, 5, 589–601, doi:10.5194/tc-5-589-2011, 2011.

TCD
9, 4625–4660, 2015

Wientjes, I. G. M., De Van Wal, R. S. W., Schwikowski, M., Zapf, A., Fahrni, S., and Wacker, L.: Carbonaceous particles reveal that Late Holocene dust causes the dark region in the western ablation zone of the Greenland ice sheet, J. Glaciol., 58, 787–794, 2012.

TCD
9, 4625–4660, 2015

Table 1. Energy inputs in 2010 and 2012.

Energy inputs – 0 to 1850 m a.s.l.	2010	2012	% difference, 2012–2010
Normalized PDDs	103	108	5
Calculated available energy for melt during the two years using a full energy balance model (TW)	2.13×10^6	2.20×10^6	3

TCD
9, 4625–4660, 2015

Table 2. Melt contributions (km^3) from different elevation intervals integrated through end of melt season, 1 October each year.

	2010	2012	% Difference
Below mean ELA	5.7	5.4	−5
1550 to 1850 m	0.5	1.1	106
1850 to 2050 m	0.1	0.4	231
Total – up to 1850 m	6.3	6.5	4
Total – up to 2050 m	6.4	7.0	9
% above MEAN ELA (1550 to 2050 m)	10.5	22.3	112
Measured proglacial discharge at 15 Sep	5.3	6.8	28
Integrated melt up 1850 m – measured discharge	1.0	−0.3	−130
integrated melt up 2050 m – measured discharge	1.1	0.2	−86

TCD
9, 4625–4660, 2015

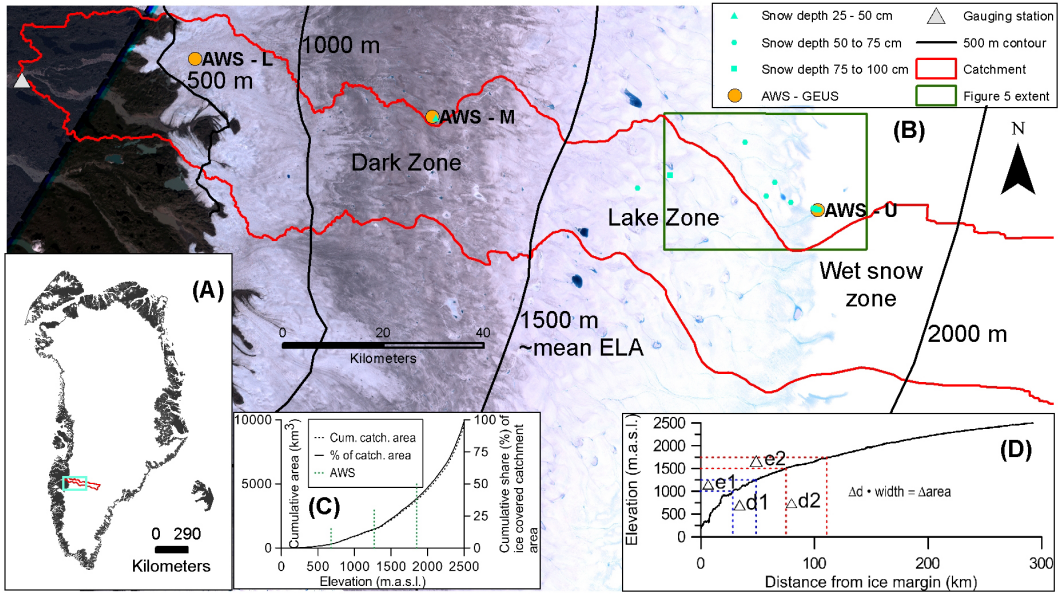

Figure 1. (a) The location of the study area (cyan) and catchment (red) in Greenland is shown on the inset map. **(b)** Map of the study area overlain with the location of the AWS, gauging station, catchment area, and snow pit sites. The background Landsat 7 image, which was acquired on 16 July 2012, reveals surface water in lakes and streams occurred at an exceptional and unprecedented elevation of ~ 1840 m a.s.l. The non-linear increase in the size of the catchment with increasing elevation is shown in **(c)** and **(d)** shows an example of the impact on melt area with a rise in the snow line of 250 m with a 500 m displacement in different start elevations (hypsometric effect).

TCD
9, 4625–4660, 2015

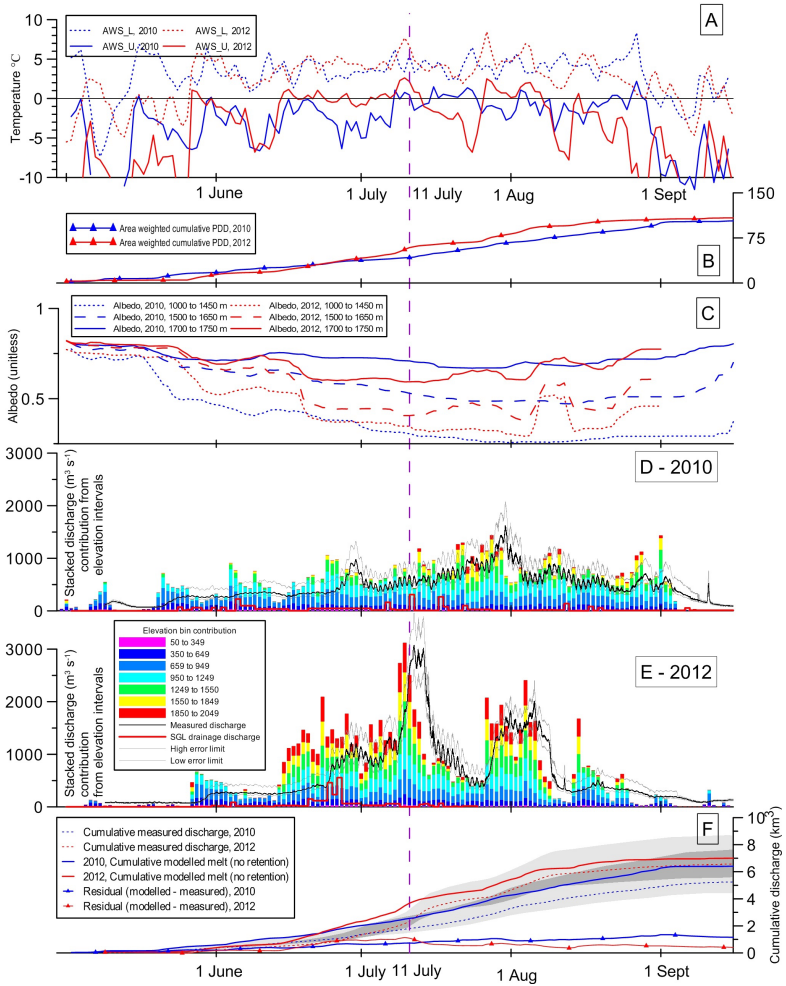

TCD
9, 4625–4660, 2015

Extraordinary runoff from the Greenland Ice Sheet in 2012

A. B. Mikkelsen et al.

Figure 2. Meteorological records, discharge measurements and modelled melt runoff for the study area during 2010 and 2012, including **(a)** daily average air temperature at AWS_L and AWS_U. (To avoid cluttering the plot the air temperature at AWS_U is only plotted during summer and the air temperature at AWS_M, which usually les between that of AWS_L and AWS_U is not plotted at all). **(b)** the area weighted cumulative PDD, **(c)** the albedo at three different elevation bands, **(d, e)** the proglacial discharge, supraglacial lake drainage volume, and modelled melt runoff, and **(f)** the cumulative proglacial discharge, modelled melt runoff, and residual between the two. The dashed vertical purple line demarks the bridge wash out on 11 July 2012. The uncertainty in discharge estimates is shown using grey lines on **(d)** and **(e)** and by grey shading on **(f)**. Where the uncertainty estimates for 2010 and 2012 overlap on **(f)** a darker shade of grey is used.

TCD
9, 4625–4660, 2015

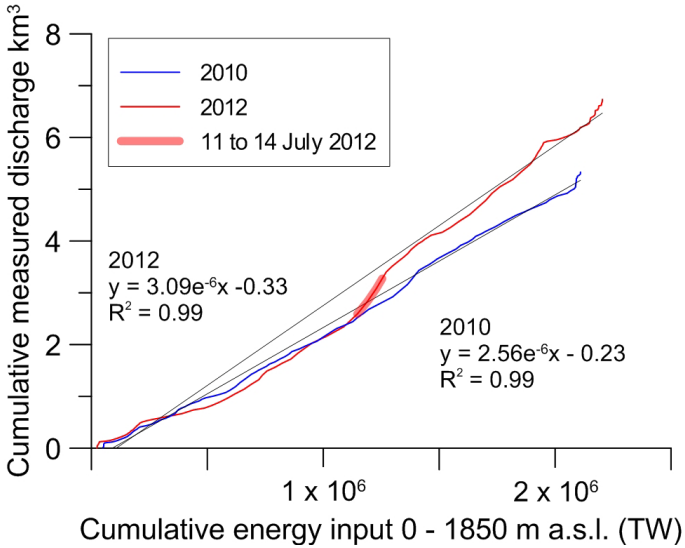

Figure 3. The cumulative measured discharge as a function of the calculated energy input for the catchment up to 1840 m a.s.l. The flooding period of 11 to 14 July is marked with a bold red line.

TCD
9, 4625–4660, 2015

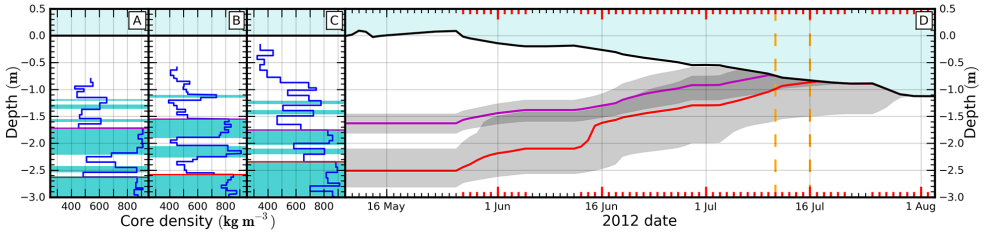

Figure 4. (a–c) Density profiles of three shallow firn cores (**a–c** respectively) drilled at AWS_U in May 2012. The water table is indicated in light blue and ice lenses observed in the core straigraphy are indicated in cyan. Magenta and red lines indicate two potential sets of "blocking" ice lenses observed in the firn. **(d)** A model simulation of the near-surface water table at AWS_U for each of the two blocking lens assumptions in **(a–c)**, with 95 % confidence intervals in grey. Red ticks on the horizontal axes indicate days above freezing when surface melt would occur. As snow melts above the blocking lenses the water table rises simultaneously until it meets the lowering snow surface. Light blue is free air. The daily snow surface is observed by the adjacent AWS_U AWS. The two dashed orange vertical lines indicate 11 July, the date of the Watson River bridge destruction, and 16 July, when the Landsat image from Fig. 1 shows horizontal water transport in the vicinity of AWS_U.

TCD
9, 4625–4660, 2015

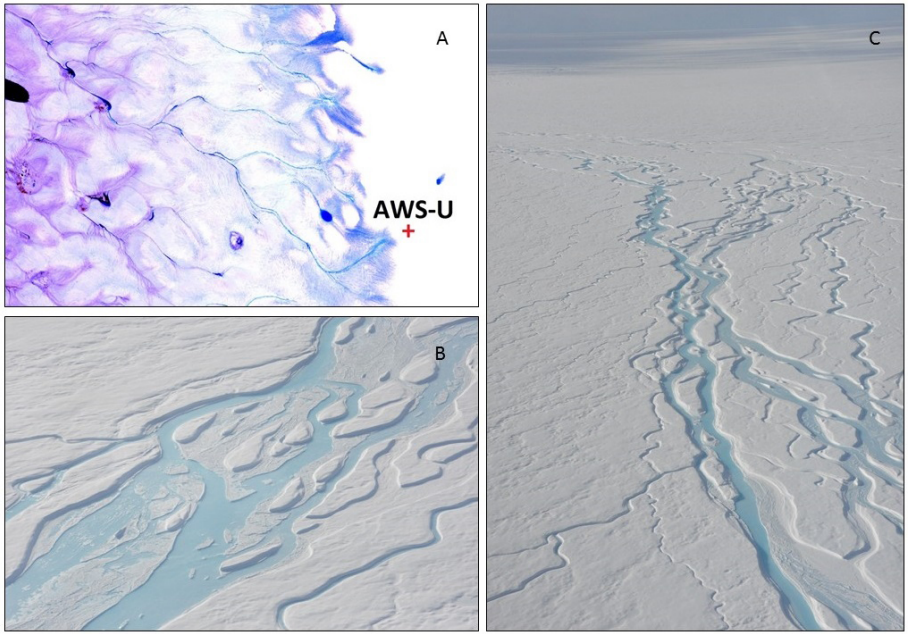

Figure 5. (a) Zoom in on Landsat 7 image from 16 July 2012 showing free surface water in the area around AWS_U. The extent is marked on Fig. 1. The scan line correction failure was interpolated using the ENVI "replace bad data" routine based on Band 8 and visible surface water was enhanced using a modified normalized difference water index (Fitzpatrick et al., 2014). (**b** and **c**) Oblique aerial photographs of the active surpraglacial channel netowk emerging from AWS_U well within the accumulation zone at 1840 m a.s.l. and 140 km from the ice sheet margin on 13 August 2012. Courtesy of Paul Smeets.

TCD
9, 4625–4660, 2015